[CANCER RESEARCH 64, 5760–5766, August 15, 2004]

Induction of Morphological and Biochemical Apoptosis following Prolonged Mitotic Blockage by Halichondrin B Macrocyclic Ketone Analog E7389

Galina Kuznetsov,[1] Murray J. Towle,[2] Hongsheng Cheng,[2] Takanori Kawamura,[6] Karen TenDyke,[1] Diana Liu,[2] Yoshito Kishi,[5] Melvin J. Yu,[3] and Bruce A. Littlefield[4]

Departments of [1]Candidate Assessment and In Vitro Technologies, [2]Life Sciences, [3]Lead Optimization, [4]Scientific Administration, and [5]Advisory Board, Eisai Research Institute, Andover, Massachusetts, and [6]Discovery Research Laboratories II, Tsukuba Research Laboratories, Eisai Company, Ltd., Tsukuba-shi, Ibaraki, Japan

ABSTRACT

E7389, a macrocyclic ketone analog of the marine natural product halichondrin B, currently is undergoing clinical trials for cancer. This fully synthetic agent exerts its highly potent *in vitro* and *in vivo* anticancer effects via tubulin-based antimitotic mechanisms, which are similar or identical to those of parental halichondrin B. In an attempt to understand the impressive potency of E7389 in animal models of human cancer, its ability to induce apoptosis following prolonged mitotic blockage was evaluated. Treatment of U937 human histiocytic lymphoma cells with E7389 led to time-dependent collection of cells in the G_2-M phase of the cell cycle, beginning as early as 2 h and becoming maximal by 12 h. Increased numbers of hypodiploid events were seen beginning at 12 h, suggesting initiation of apoptosis after prolonged E7389-induced mitotic blockage. The identity of hypodiploid events as apoptotic cells under these conditions was confirmed by two additional morphologic criteria: green to orange/yellow shifts on acridine orange/ethidium bromide staining, and cell surface annexin V binding as assessed by flow cytometry. Several biochemical correlates of apoptosis also were seen following E7389 treatment, including phosphorylation of the antiapoptotic protein Bcl-2, cytochrome *c* release from mitochondria, proteolytic activation of caspase-3 and -9, and cleavage of the caspase-3 substrate poly(ADP-ribose) polymerase (PARP). In LNCaP human prostate cancer cells, treatment with E7389 also led to generation of hypodiploid cells, activation of caspase-3 and -9, and appearance of cleaved PARP, indicating that E7389 can activate cellular apoptosis pathways under anchorage-independent and -dependent cell culture conditions. These results show that prolonged mitotic blockage by E7389 can lead to apoptotic cell death of human cancer cells *in vitro* and can provide a mechanistic basis for the significant *in vivo* anticancer efficacy of E7389.

INTRODUCTION

Halichondrin B (Fig. 1) is a large polyether macrolide originally isolated from the marine sponge *Halichondria okadai* (1, 2). In the mid-1980s, halichondrin B was shown to have extremely potent anticancer activities (1, 2), which subsequently were shown to be based on a microtubule-destabilizing antimitotic mechanism of action (3). Although several other anticancer agents, such as *Vinca* alkaloids, dolastatins, and cryptophycin, share this mechanism, interactions between halichondrin B and tubulin were found to be unique compared with other tubulin agents (3–6), suggesting that halichondrin B-based anticancer drugs might have a unique spectrum of clinical activities.

Despite its remarkable *in vitro* and *in vivo* anticancer activities, natural halichondrin B was not readily available in quantities sufficient for drug development purposes. Fortunately, achievement of the complete chemical synthesis of halichondrin B (7), together with the discovery that its biological activity resides in its macrocyclic lactone C.1–C.38 ("right half") moiety[7] (see also Refs. 8–10), provided a realistic opportunity for drug development based on the renewable resource of chemical synthesis. A series of structurally simplified and chemically stabilized synthetic analogs of the right half of halichondrin B was developed (10), with compound E7389 (NSC 707389, previously ER-086526; Fig. 1) ultimately chosen as a clinical candidate (11). E7389 currently is undergoing clinical trials for cancer.

Similar to parental halichondrin B, E7389 induces mitotic blocks in cancer cells via mitotic spindle disruption secondary to inhibition of tubulin polymerization (11). E7389 inhibits proliferation of a wide variety of human cancer cell types at subnanomolar concentrations and shows impressive anticancer activity against several human cancer xenograft models *in vivo*, including frank regressions and cures (11). In an attempt to better understand the anticancer mechanism of action of E7389, its ability to induce apoptosis in human cancer cells *in vitro* was evaluated. In this study, induction of apoptosis following prolonged mitotic blockage by E7389 is shown by several key morphologic and biochemical criteria, providing a mechanistic basis for the anticancer effects of E7389.

MATERIALS AND METHODS

Cell Culture and E7389 Treatment. U937 human histiocytic lymphoma cells and LNCaP human prostate cancer cells were obtained from American Type Culture Collection (Manassas, VA) and maintained in suspension or monolayer cultures, respectively, in RPMI 1640 medium supplemented with 10% fetal bovine serum. Details of cell culture conditions for these two lines have been described previously (11). E7389 was chemically synthesized as described (12), prepared as 1 mM stocks in 100% DMSO, and stored in small aliquots at −80°C until use. Cells were treated with E7389 for the indicated time periods following appropriate sterile dilution of DMSO stock solutions into tissue culture medium. Final DMSO concentrations during treatment of cells did not exceed 0.1% (v/v). E7389 was used at 100 nM, a concentration roughly 10-fold higher than that required to minimally induce complete G_2-M cell cycle blocks based on dose-response studies.

Flow Cytometric Cell Cycle Analysis. After treatment with 100 nM E7389 for 0–24 h (U937) or 0–48 h (LNCaP), cells were harvested by low-speed centrifugation, fixed in 70% (v/v) ethanol, treated with RNase, stained with propidium iodide (PI), and subjected to single-channel flow cytometry for determination of cell cycle characteristics. Details of fixation procedures and flow cytometry have been described previously (11). Flow cytometry was performed on a Becton Dickinson FACScan (Franklin Lakes, NJ), with collection and analysis of data performed using Becton Dickinson CELLQuest software.

Acridine Orange/Ethidium Bromide Staining. U937 cells were incubated with or without 100 nM E7389 for 24 h. Cells were harvested by centrifugation, exposed to 40 μg/ml acridine orange (Sigma, St. Louis, MO) plus 100 μg/ml ethidium bromide (Bio-Rad, Hercules, CA), and visualized by fluorescence microscopy using a Nikon Diaphot inverted microscope (Tokyo, Japan). Cells were not fixed or permeabilized before dye exposure.

Annexin V/PI Flow Cytometric Staining Techniques. U937 cells were incubated with or without 100 nM E7389 for 0–24 h. Cells were harvested by low-speed centrifugation, washed twice in PBS, and resuspended in binding buffer [10 mM HEPES (pH 7.4), 140 mM NaCl, 2.5 mM $CaCl_2$; BD PharM-

Received 4/3/04; revised 5/25/04; accepted 6/14/04.

The costs of publication of this article were defrayed in part by the payment of page charges. This article must therefore be hereby marked *advertisement* in accordance with 18 U.S.C. Section 1734 solely to indicate this fact.

Note: These data were presented in part (abstract 1318) at the 93rd Annual Meeting of the AACR held April 6–10, 2002, San Francisco, CA.

Requests for reprints: Bruce A. Littlefield, Eisai Research Institute, 4 Corporate Drive, Andover, MA 01810-2441. Phone: 978-837-4638; Fax: 978-794-4910; E-mail: bruce_littlefield@eri.eisai.com.

[7] M. J. Towle, Y. Kishi, and B. A. Littlefield, unpublished observations, 1992.

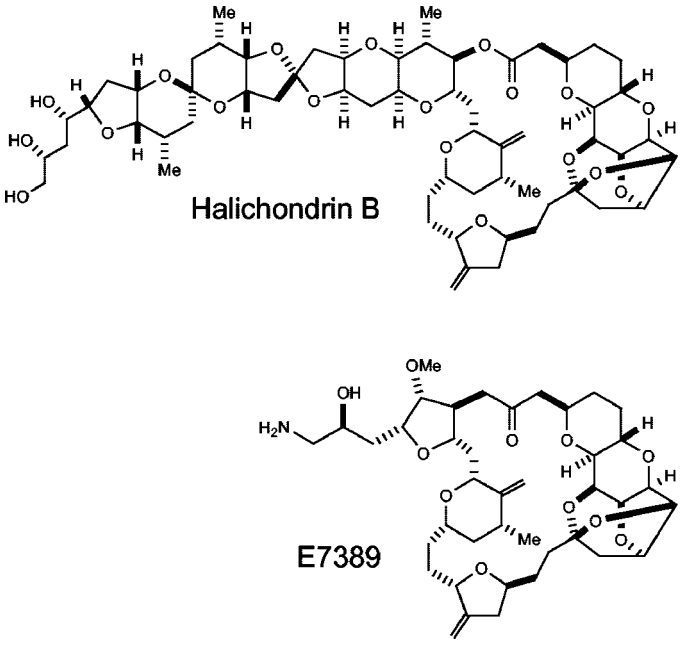

Fig. 1. Structures of halichondrin B and E7389

ingen, San Diego, CA] at 10^6 cells/ml. FITC-conjugated annexin V and PI (both from BD PharMingen) were added at manufacturer's recommended concentrations to 0.1 ml aliquots containing 10^5 cells. Cells were incubated for 15 min at 18°C in the dark. Cell suspensions were diluted with 0.4 ml binding buffer and analyzed by flow cytometry within 1 h. Flow cytometry was performed on a Becton Dickinson FACScan, with collection and analysis of data performed using Becton Dickinson CELLQuest software.

Preparation of Whole Cell Lysates and Immunoblot Analyses. Cells were harvested by gentle scraping and/or centrifugation and lysed in Laemmli's SDS sample buffer (13) containing a protease inhibitor mixture [containing 4-(2-aminoethyl)-benzenesulfonylfluoride, aprotinin, bestatin, E-64, leupeptin hemisulfate, and pepstatin A; Calbiochem, San Diego, CA], 1 mM phenylmethylsulfonyl fluoride, 20 μM caspase inhibitor z-Val-Ala-Asp-fluoromethyl ketone (z-VAD-FMK), and 50 mM DTT. Cell lysates were heated to 100°C for 10 min and subjected to SDS-PAGE, followed by Western blot analysis with various apoptosis-related antibodies. Bcl-2 antibody clone 124 was purchased from DAKO (Glostrup, Denmark; catalogue no. M 0887). Two poly(ADP-ribose) polymerase (PARP) antibodies were used: mouse monoclonal anti-PARP antibody, which recognizes the uncleaved (M_r 116,000) and cleaved (M_r 85,000) fragments of PARP (BD PharMingen; catalogue no. 556494), and PARP anticleavage site antibody (BioSource International, Camarillo, CA; catalogue no. 44–699). Anti-cytochrome *c* antibody was purchased from BD PharMingen (catalogue no. 65981A).

Preparation of Postmitochondrial Fraction Lysates. U937 cells were collected by low-speed centrifugation and allowed to swell in a detergent-free hypotonic buffer [220 mM mannitol, 68 mM sucrose, 50 mM PIPES (pH 7.4), 50 mM KCl, 4 mM EGTA, 2 mM $MgCl_2$, and 1 mM DTT] containing protease inhibitor mixture (Calbiochem; see previous section), 1 mM phenylmethylsulfonyl fluoride, and 50 μl z-VAD-FMK for 30 min on ice. Cells were gently homogenized using a loose ("B" pestle) Dounce homogenizer and centrifuged at 15,000 $\times$ *g* for 30 min at 4°C to remove mitochondria. Resulting supernatant devoid of mitochondria (postmitochondrial fraction) was lysed in Laemmli's SDS sample buffer containing 50 mM DTT and heated to 100°C for 10 min (referred to as postmitochondrial lysate). Whole cell lysates and postmitochondrial lysates were subjected to SDS-PAGE, followed by Western blot analysis with anti-cytochrome *c* antibody (BD PharMingen).

Caspase Activity Measurements. U937 and LNCaP cells were treated with 100 nM E7389 for 0–24 h. Caspase-3 activation was measured using a caspase-3 colorimetric assay kit (ApoAlert; Clontech, Palo Alto, CA). Sample sizes were 2×10^6 U937 cells or 1.8×10^6 LNCaP cells. Generation of the chromophore *p*-nitroanilide following cleavage of the chromogenic caspase-3 substrate was monitored colorimetrically by absorbance at 405 nm. Caspase-9 activation was measured using a caspase-9 fluorometric assay kit (Oncogene Research Products, Boston, MA). Sample sizes of 1×10^6 cells were used. A blue to green shift in fluorescence indicated generation of the fluorophore 7-amino-4-trifluoromethyl coumarin following cleavage of the fluorogenic caspase-9 substrate. Culture medium samples at 0 h and 24 h were used as negative controls in the caspase-3 and -9 assays. A U937 cell lysate preincubated with the caspase-9 inhibitor benzoxyl carbonyl-leu-glu (OMe)-his-asp(OMe)-fluoromethylketone (z-LEHD-FMK) also was included as a negative control in the caspase-9 assay.

RESULTS

E7389 Induces G_2-M Arrest and Appearance of Hypodiploid Cells. Previous studies have shown E7389 to be a potent tubulin-based antimitotic agent (11). To investigate whether this activity was associated with induction of apoptosis in cancer cells, flow cytometric cell cycle analysis of exponentially growing U937 histiocytic lymphoma cells treated with 100 nM E7389 for 0–24 h was performed. As shown in Fig. 2*A*, untreated (0 h) cells show a typical pattern of

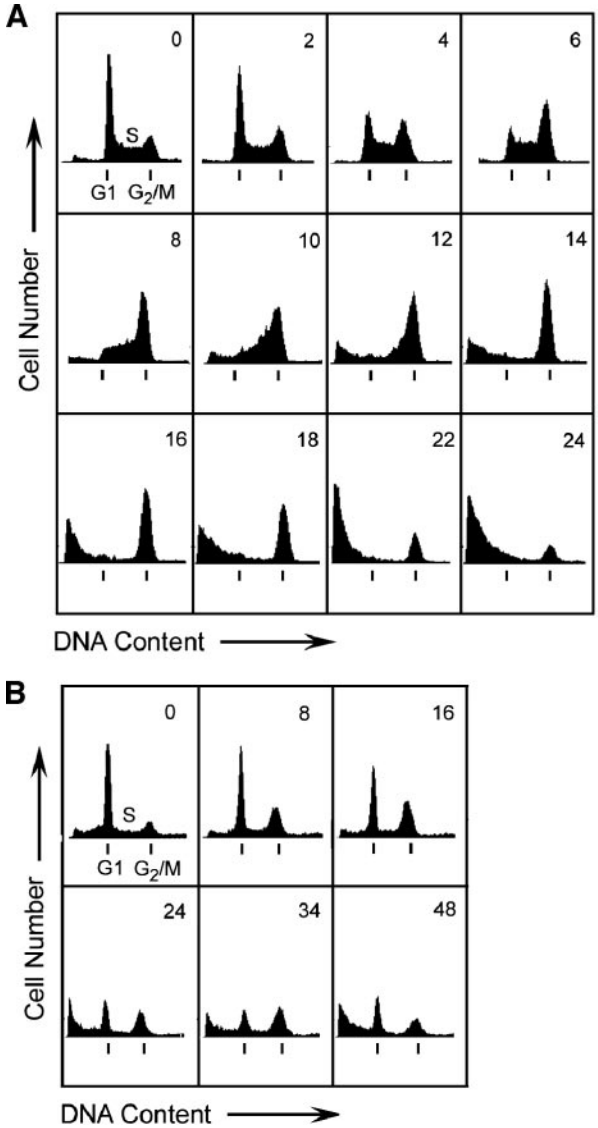

Fig. 2. E7389 induces G_2-M blocks and appearance of hypodiploid cells in U937 histiocytic lymphoma and LNCaP prostate cancer cells. Histograms show number of cells per channel (*vertical axis*) *versus* DNA content (*horizontal axis*). U937 cells (*A*) and LNCaP cells (*B*) were treated with 100 nM E7389 for 0–24 h or 0–48 h, respectively, followed by staining with PI and flow cytometric cell cycle analysis as described in "Materials and Methods."

randomly cycling cells distributed across the G_1 (53%), S (20%), and G_2-M (17%) phases. Treatment with E7389 induced G_2-M blocks beginning as early as 2 h and increasing continuously until the maximal block was achieved at 12 h. Between 8 h and 12 h, the percentage of cells in G_2-M reached the highest levels (60–63%); after 12 h, this percentage began to decrease. Beginning at 10 h, increased numbers of hypodiploid (sub-G_1) events were seen, suggesting that cells were undergoing apoptosis after prolonged mitotic blockage and accounting for the steadily decreasing G_2-M populations seen after 12 h. By 24 h of E7389 exposure, most events (73%) occurred in the hypodiploid population, presumably representing apoptotic cells (14). In separate experiments, analysis of phospho-histone H3 levels, a marker for mitosis (15), indicated that at least 83–87% of U937 cells collected in G_2-M peaks at 12 h and 16 h were actually in mitosis (data not shown). Importantly, hypodiploid cells were seen to derive directly and exclusively from the phospho-histone H3-positive G_2-M population, indicating that the source of hypodiploid cells was directly from mitotic cells (data not shown).

To investigate whether induction of apoptosis by E7389 occurs under anchorage-independent and -dependent cell culture conditions, we used human prostate cancer LNCaP cells, which grow as a monolayer culture. As shown in Fig. 2*B*, E7389 effects on LNCaP cells were similar to those seen in U937 suspension cultures because treatment with 100 nM E7389 resulted in G_2-M blockage and generation of significant numbers of hypodiploid events. The growth rate of LNCaP cells is significantly slower than that of U937 cells, accounting for the fact that cell cycle effects seen in LNCaP cells are significantly slower than those seen in U937 cells. Thus, the beginning of G_2-M arrest in LNCaP cells was only just evident at 8 h, with full G_2-M blockage still not occurring even at 48 h. At 24 h, the percentage of cells in G_1 had decreased to 14% from the 47% seen in untreated cells, whereas percentages in the G_2-M phase increased from 14% to 22%. Also at 24 h, significantly increased numbers of hypodiploid events were seen (17% of total events), suggesting that, like U937 cells in suspension culture, LNCaP cells in monolayer culture undergo processes consistent with apoptosis following prolonged E7389-induced mitotic blocks. Interestingly, unlike U937 cells, a G_1 phase peak persisted in E7389-treated LNCaP cells for up to 48 h, similar to reports of G_1 arrest by microtubule agents via p53/p21-dependent processes (16, 17). In this regard, it is noteworthy that paclitaxel has been shown to induce p53/p21 in LNCaP cells (18).

Morphologic Evidence for E7389-Induced Apoptosis. The hypodiploid events seen in flow cytometric analyses of E7389-treated U937 cultures suggested induction of apoptosis following prolonged mitotic blocks. This was confirmed morphologically via staining of unfixed, nonpermeabilized cells with the DNA-intercalating fluorescent dyes acridine orange and ethidium bromide (19, 20). Acridine orange is cell permeable and can enter healthy or dying cells. Ethidium bromide can only enter dead or dying cells in which cell membrane integrity is compromised. Combination of the two dyes in the same cell results in a color shift from green/yellow to orange/red (19, 20). Fig. 3 shows U937 cells after 24-h treatment without (*A*) or with (*B*) 100 nM E7389. In contrast to the bright green/yellow staining of healthy control cells (Fig. 3*A*), E7389 treatment induced a pronounced shift to orange/red staining (Fig. 3*B*). Extensive nuclear condensation and fragmentation, known characteristics of apoptotic cells, simultaneously were noted in E7389-treated cultures (Fig. 3*B*). Together with the presence of hypodiploid cells seen in flow cytometric analyses, these morphologic observations confirm the presence of apoptotic cell death following prolonged E7389-induced mitotic blocks.

E7389 Induces Loss of Plasma Membrane Polarity. One of the earliest events of apoptosis is loss of plasma membrane polarity, which is accompanied by translocation of phosphatidylserine (PS) from the inner to outer membrane leaflets, thereby exposing PS to the external environment (21, 22). The phospholipid-binding protein annexin V has a high affinity for PS and can bind to cells with externally exposed PS. Positive staining with fluorescently labeled annexin V correlates with loss of membrane polarity but precedes the complete loss of membrane integrity that accompanies later stages of cell death resulting from either apoptosis or necrosis (21, 22). In contrast, PI can only enter cells after loss of membrane integrity. Thus, dual staining with annexin V and PI allows clear discrimination between unaffected cells (annexin V negative, PI negative), early apoptotic cells (annexin V positive, PI negative), and late apoptotic cells (annexin V positive, PI positive).

Using this technique, progressive transitioning of E7389-treated U937 cells from largely unaffected (0–8 h) through early apoptosis (10–16 h) to late stage apoptosis (18–24 h) is clearly seen (Fig. 4). In this study, cells remained largely unaffected for the first 6 h of E7389 treatment, with the small percentage of apoptotic cells representing background levels of apoptosis that characterize healthy cell populations. This was followed by the appearance of early apoptotic cells at 8 h; this population then increased rapidly between 8–12 h. Late-stage apoptotic cells began to appear at 12 h, followed by increases in this population until maximal values were reached at 22 h. An interesting aspect of this study is that after the initial increases in early apoptotic cells (8–12 h), no further changes in this population occurred because

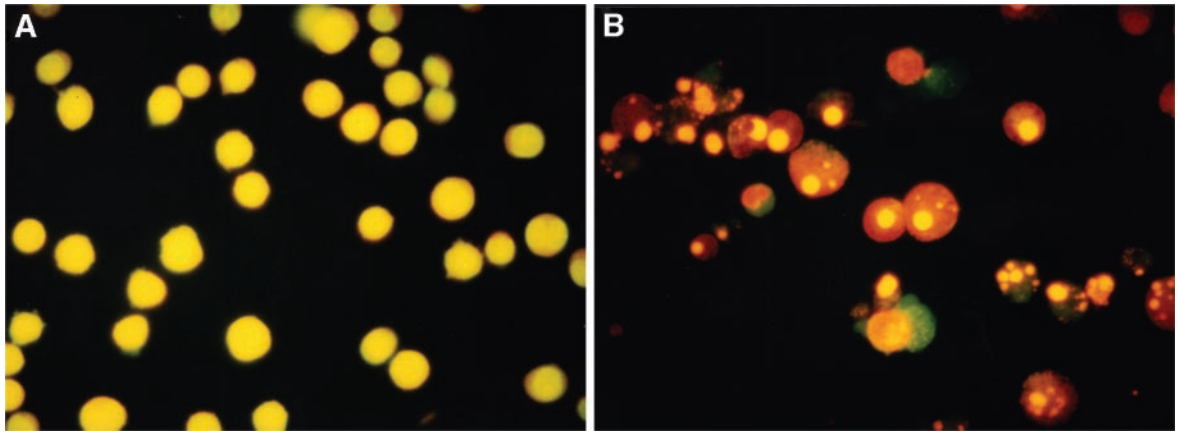

Fig. 3. Morphologic evidence of apoptosis in E7389-treated U937 cells. U937 cells were incubated in the absence (*A*) or presence (*B*) of 100 nM E7389 for 24 h. Cells were stained with acridine orange/ethidium bromide and visualized by fluorescence microscopy using a blue filter as described in "Materials and Methods."

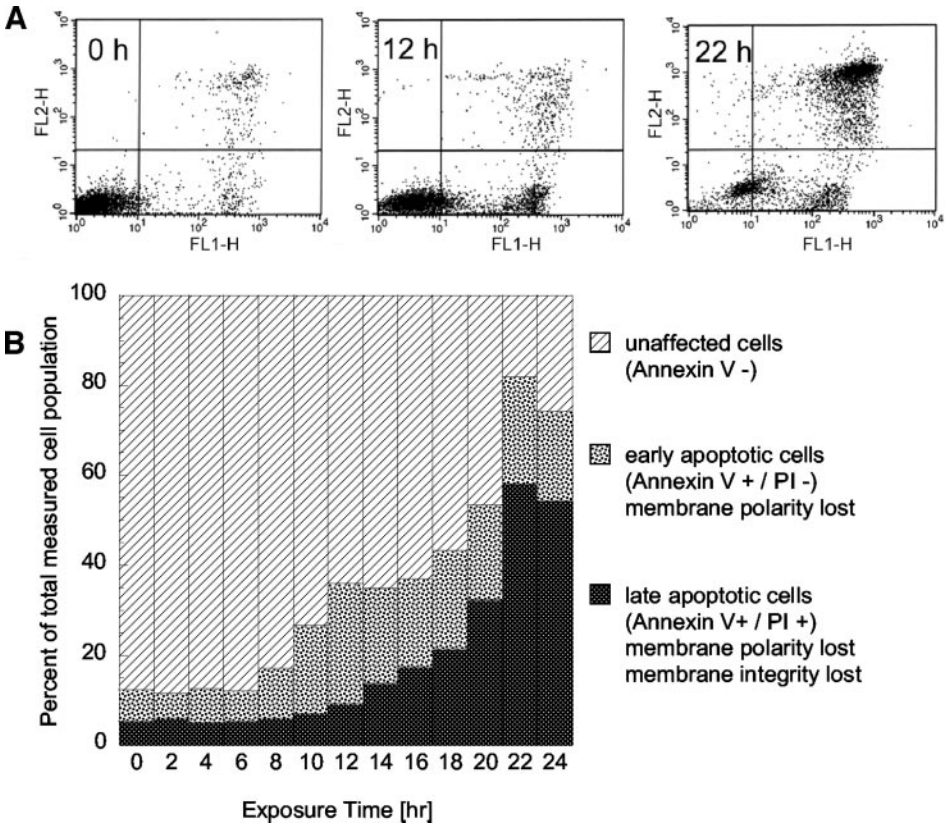

Fig. 4. E7389 triggers U937 cell surface PS expression before loss of membrane integrity. U937 cells were treated with 100 nM E7389 for 0–24 h, stained with annexin V and PI, and analyzed by flow cytometry. *A*, examples of flow cytometric analysis at 0, 12, and 22 h of treatment. The horizontal (*FL1-H*) and vertical (*FL2-H*) axes represent labeling with annexin V and PI, respectively. Bottom left quadrant represents live cells (annexin V negative, PI negative); bottom right quadrant represents early apoptotic cells (annexin V positive, PI negative); and top right quadrant represents late apoptotic cells (annexin V positive, PI positive). *B*, percentages of the total cell population are plotted for normal healthy cells (annexin V negative, PI negative), early apoptotic cells (annexin V positive, PI negative), and late apoptotic cells (annexin V positive, PI positive). Details of all of the procedures are presented in "Materials and Methods."

early apoptosis is transient, with cells continually traversing this phase before moving into late-stage apoptosis.

E7389 Induces Bcl-2 Phosphorylation. Bcl-2 is an antiapoptotic protein whose function is regulated by phosphorylation (23, 24). Induction of mitotic arrest by microtubule active agents leads to multisite phosphorylation and inactivation of Bcl-2, followed by initiation of apoptosis (25–27). To determine whether this mechanism contributes to E7389-induced apoptosis, we examined time-dependent changes in Bcl-2 phosphorylation in E7389-treated U937 cells. As shown in Fig. 5*A*, Bcl-2 phosphorylation (slower-migrating bands on SDS-PAGE) was detected after only 2 h of E7389 treatment, a time which corresponds to the earliest detection of G_2-M block by flow cytometry (Fig. 2). A ladder of slower-migrating Bcl-2 bands was detected beginning at 4 h, indicating multiple phosphorylation events triggered by E7389 treatment. The intensity and number of phosphorylated bands peaked at ~10 h, a time roughly corresponding to the maximal G_2-M block but before substantial accumulation of apoptotic cells as assessed by hypodiploid cell numbers and staining patterns with acridine orange/ethidium bromide, annexin V, and PI (Figs. 2–4). The intensity and number of Bcl-2 phosphorylated bands then decreased between 12–24 h, a time of rapidly increasing numbers of dead and dying cells as judged by the flow cytometric and morphologic criteria described previously.

E7389 Triggers Release of Mitochondrial Cytochrome *c*. In apoptosis triggered by most chemotherapeutic agents, mitochondrial cytochrome *c* is released to the cytosol, where it promotes assembly of the apoptosome and activation of caspase-9, which then triggers additional downstream apoptotic events, including activation of effector caspase-3 and -7 (28–31). To gauge the contribution of this pathway to apoptosis induction by E7389, U937 cells were treated with 100 nM E7389 for 2, 4, 8, and 16 h, followed by preparation of whole cell and postmitochondrial lysates, which then were analyzed by SDS-PAGE and Western blot analysis with anti-cytochrome *c* antibodies. Fig. 5*B* shows that, as expected, cytochrome *c* is present in all of the whole cell lysates (*bottom*) but is seen only at extremely low levels in postmitochondrial lysates from untreated cells (*top*, *right*). Similarly, cytochrome *c* is not detected in postmitochondrial lysates from cells treated with E7389 for only 2–4 h (Fig. 5*B*, *top*, *left*). In contrast, large amounts of cytochrome *c* were detected in postmitochondrial lysates from cells treated with E7389 for 8 h or 16 h (Fig. 5*B*). These results show E7389 triggered release of mitochondrial cytochrome *c* in a timeframe that corresponds to onset of apoptosis by the several morphologic criteria discussed previously. Onset of cytochrome *c* release at 8 h also corresponds well with the time of maximal Bcl-2 phosphorylation levels as seen previously (Fig. 5*A*).

E7389 Treatment Leads to Activation of Caspase-3 and -9. Caspase-9 is activated on release of cytochrome *c* from mitochondria. Activated caspase-9 then proteolytically activates other caspases, including the effector caspase-3 and -7, thus initiating a caspase activation cascade leading to apoptosis (32–35). On the basis of this knowledge and the observation of E7389-induced cytochrome *c* release, activities of caspase-3 and -9 were examined to determine the involvement of this pathway in E7389-induced apoptosis. As shown in Fig. 6, activities of caspase-3 and -9 increased in a time-dependent manner following exposure of U937 and LNCaP cells to E7389. Moreover, the specific caspase-9 inhibitor z-LEHD-FMK (36) blocked increased caspase-9 activity in U937 cells. These data support the involvement of caspase-3 and -9 as mediators of E7389-induced apoptosis.

E7389 Treatment Causes Proteolytic Cleavage of PARP. The nuclear DNA repair enzyme PARP is a target of caspase-3, and its cleavage can serve as a biochemical marker of apoptosis (37, 38). Therefore, we tested whether E7389-induced apoptosis is associated with PARP cleavage, which is detectable by the appearance of an M_r 84,000 cleavage fragment on SDS-PAGE. As shown in Fig. 5*C*, time-dependent PARP cleavage was seen in U937 and LNCaP cells

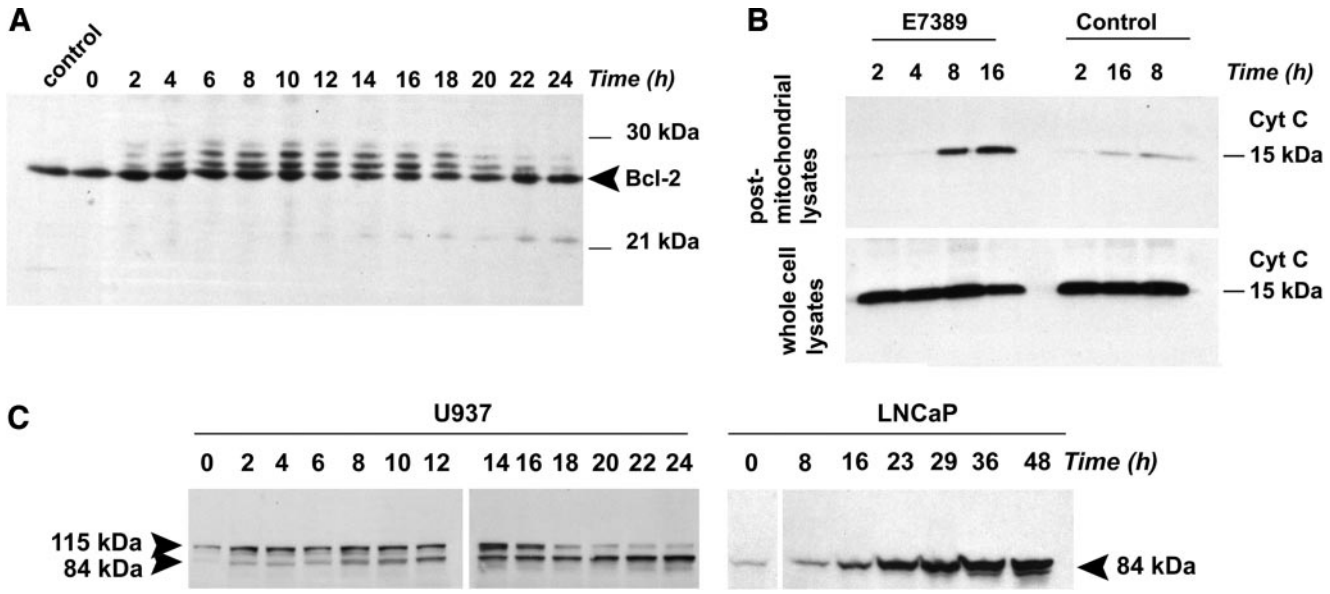

Fig. 5. E7389 treatment leads to Bcl-2 phosphorylation, mitochondrial cytochrome *c* release, and PARP cleavage. *A*, Bcl-2 phosphorylation. U937 cells were incubated with 100 nM E7389 for 0–24 h. Total cell lysates were subjected to 10% SDS-PAGE, followed by Western immunoblot analysis using anti-Bcl-2 antibodies. Rapid phosphorylation of Bcl-2 is evident by appearance of slower (higher) migrating bands as early as 2 h after the beginning of E7389 treatment. *B*, mitochondrial cytochrome *c* release. U937 cells were treated with 100 nM E7389 for 2, 4, 8, and 16 h. At the end of each treatment period, cells were collected by centrifugation. Cell samples were divided into two aliquots: one for preparation of whole cell lysates, and the other for preparation of postmitochondrial lysates. Lysates were subjected to 4–20% gradient SDS-PAGE, followed by Western immunoblot analysis with anti-cytochrome *c* antibodies. Cytochrome *c* is seen as a band migrating at M_r 15,000. *Top*, Western blot analysis of mitochondria-free lysates. *Bottom*, Western Blot analysis of whole cell lysates. *C*, PARP cleavage. U937 cells and LNCaP cells were treated with 100 nM E7389 for the indicated time periods. An anti-PARP antibody that recognizes the uncleaved (M_r 115,000) and cleaved (M_r 84,000) PARP polypeptides was used in the Western blot analysis of E7389-treated U937 cells (*left*). An anti-PARP antibody that recognized only the cleaved (M_r 84,000) PARP polypeptide was used in the Western blot analysis of E7389-treated LNCaP cells (*right*).

after E7389 treatment. The anti-PARP antibody used in the U937 experiment (Fig. 5*C*, *left*) recognizes uncleaved and cleaved PARP (M_r 115,000 and 84,000, respectively), whereas the antibody used in the LNCaP experiment recognizes only cleaved PARP (M_r 84,000; Fig. 5*C*, *right*). In both cell lines, significant PARP cleavage was detected by 8 h of treatment with E7389. In U937 cells, PARP cleavage was essentially complete by ~18–20 h of treatment. In LNCaP cells, it was not possible to determine when uncleaved PARP was depleted because the antibody used in this experiment only recognized cleaved PARP. However, cleaved PARP appeared to continue to accumulate even as late as 36–48 h, suggesting this process was slower in LNCaP cells compared with U937 cells. This interpretation is consistent with earlier observations that G_2-M block setup and apoptosis induction were slower in LNCaP cells compared with U937 cells.

DISCUSSION

In this study, we showed that treatment of U937 and LNCaP cells with E7389 led to time-dependent collection of cells in the G_2-M phase of the cell cycle, results which agree with our previous characterization of E7389 as a tubulin-based antimitotic agent (11). Steadily increasing numbers of hypodiploid cells seen after E7389 treatment suggested that cells began undergoing apoptosis after prolonged E7389-induced mitotic block. The presence of apoptotic U937 cells under these conditions was confirmed by two morphologic criteria: green/yellow to red/orange shifts using acridine orange/ethidium bromide staining techniques, and cell surface annexin V binding indicative of PS appearance on the external plasma membrane. Several biochemical correlates of apoptosis also were seen following E7389 treatment, including phosphorylation of Bcl-2, cytochrome *c* release from mitochondria, activation of caspase-3 and -9, and cleavage of PARP. Detection of mitochondrial cytochrome *c* release and activation of caspase-9 indicated that E7389 treatment led to activation of the so-called mitochondrial apoptotic pathway, the mechanism most commonly associated with responses to chemotherapy agents. E7389 treatment caused activation of apoptosis pathways and markers under suspension and anchorage-dependent culture conditions. Together, our results show that prolonged mitotic blockage by E7389 leads to apoptotic cell death of human cancer cells *in vitro*, thereby providing a cellular mechanistic basis for its potent anticancer effects seen *in vivo*.

The current studies do not address whether apoptosis is induced at E7389 concentrations <100 nM. However, induction of G_2-M blocks in U937 cells by treatment with ≥10 nM E7389 for 12 h followed by drug washout leads to completely nonviable cell populations 5 days later (39). These findings, together with results from the current study showing clear apoptosis induction at 100 nM, suggest that concentrations capable of inducing complete mitotic blocks (≥10 nM) also lead to induction of apoptosis.

Other agents that disrupt microtubule dynamics (*e.g.*, paclitaxel, vinblastine, and isohomohalichondrin B, a relative of E7389 parent halichondrin B), also have been reported to induce apoptosis following a mitotic arrest (25, 26, 40, 41), although the precise signaling pathways triggering apoptosis following mitotic arrest have not been completely elucidated. Recent reports suggest that tubulin-acting compounds such as paclitaxel and vinblastine may induce apoptosis by stimulating phosphorylation of Bcl-2 (23, 25, 27, 42). Our finding that E7389 exposure leads to Bcl-2 hyperphosphorylation suggests that Bcl-2 also may play a role in apoptosis induction by E7389. Phosphorylation of Bcl-2 is thought to inactivate its antiapoptotic function by inhibiting formation of Bcl-2/Bax dimers (43). Phosphorylation of Bcl-2 also occurs in normal cells during mitosis (40). Thus, Bcl-2 phosphorylation also can be viewed simply as a marker for mitosis; in this regard, its role in triggering apoptosis following treatment with tubulin-based agents may depend on various factors, including drug concentration, cell type, and malignancy status. How-

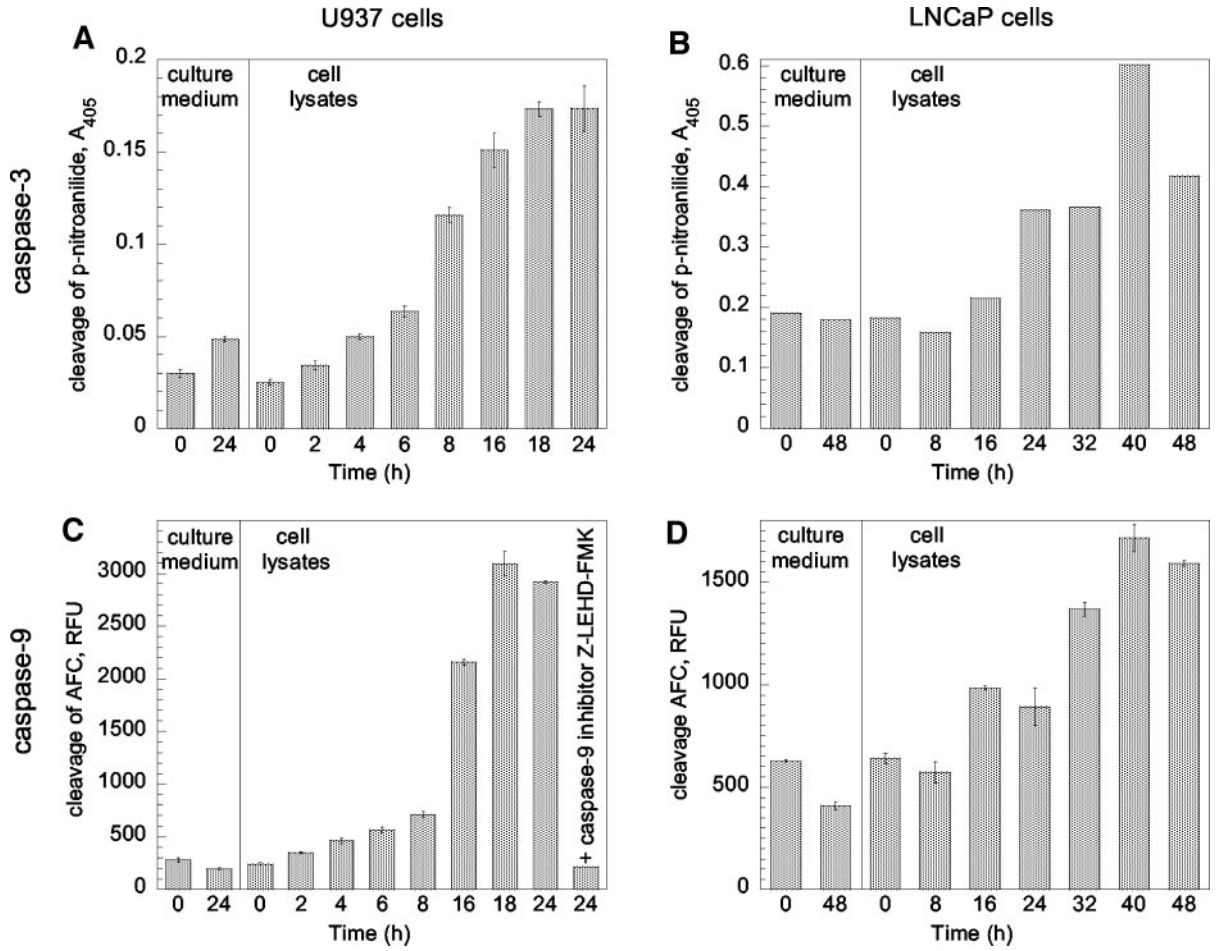

Fig. 6. E7389 treatment leads to activation of caspase-3 and -9 in U937 and LNCaP cells. U937 (*A* and *C*) and LNCaP (*B* and *D*) cells were treated with 100 nM E7389 for 0–24 h and 0-48 h, respectively. *A* and *B* show caspase-3 activation following exposure to E7389. *C* and *D* show caspase-9 activation following exposure to E7389. Culture medium samples at 0 h and 24 h (U937 cells) or 0 h and 48 h (LNCaP cells) were assayed as negative controls. A U937 cell lysate sample preincubated with the caspase-9 inhibitor z-LEHD-FMK also was included as a negative control (*C*). Details of all of the procedures are presented in "Materials and Methods."

ever, in cells destined to undergo apoptosis as a result of microtubule damage, the extent and duration of Bcl-2 phosphorylation are different, and the phosphorylation is irreversible (27, 44). Thus, prolonged G_2-M block induced by E7389 may result in persistent activation of kinases responsible for Bcl-2 phosphorylation with subsequent induction of apoptosis. Thus, this concept would be similar to the situation with paclitaxel, for which it has been proposed that Bcl-2 phosphorylation represents a suicide response to an aberrant mitotic arrest to avoid abnormal chromosome segregation (23, 45, 46).

In addition to inducing apoptosis, studies in some solid tumor cell lines have shown that microtubule-stabilizing agents, including paclitaxel, discodermolide, and epothilone, can induce a "slow cell death" through mechanisms unrelated to classical apoptosis pathways (47, 48). Therefore, it is interesting that caspase activation, PARP cleavage, and hypodiploid cells were seen at later times in LNCaP cells than in U937 cells. Thus, it is possible that the apoptotic machinery effects observed in LNCaP cells do not contribute to E7389 cytotoxicity. However, the longer times required to see such effects in LNCaP cells also may simply reflect the considerably longer cell cycle transit time of LNCaP cells compared with U937 cells. Additional studies will be required to address the relative contributions of true apoptosis and nonapoptotic "slow cell death" in E7389-treated LNCaP cells.

A number of studies have focused on identification of kinases involved in Bcl-2 phosphorylation in response to paclitaxel and vinblastine treatment. Although three c-Jun NH_2-terminal kinase phosphorylation sites on Bcl-2 have been reported (Thr69, Ser70, and Ser87; Ref. 27), the involvement of c-Jun NH_2-terminal kinase in this process remains unclear. In another study, exposure to paclitaxel and vinblastine led to concurrent activation and phosphorylation of Raf-1 kinase, suggesting the existence of a drug-induced pathway involving Raf-1 and Bcl-2 phosphorylation, with subsequent triggering of apoptosis to eliminate cells with aberrant chromosome segregation (23).

E7389 induces mitotic arrest and apoptosis in cancer cells, characteristics which are shared with several other tubulin-acting agents such as paclitaxel and vinblastine. However, the precise tubulin-based mechanisms of halichondrin B, and presumably E7389, differ significantly from other known tubulin-based agents (3–6). Thus, it is possible that the signaling pathways leading to apoptosis induction by E7389 may differ, subtly or considerably, from those of other tubulin-based agents. This will be important to establish because E7389 shows an unusually wide therapeutic window in several human xenograft cancer models *in vivo* (11), results that are consistent with a novel tubulin-based mechanism and possibly suggestive of a novel spectrum of anticancer activity in the clinic.

REFERENCES

1. Uemura D, Takahashi K, Yamamoto T, et al. Norhalichondrin A: an antitumor polyether macrolide from a marine sponge. J Am Chem Soc 1985;107:4796–8.
2. Hirata Y, Uemura D. Halichondrins: antitumor polyether macrolides from a marine sponge. Pure Appl Chem 1986;58:701–10.

3. Bai R, Paull K, Herald C, Malspeis L, Pettit G, Hamel E. Halichondrin B and homohalichondrin B marine natural products binding in the vinca domain of tubulin. Discovery of tubulin-based mechanism of action by analysis of differential cytotoxicity data. J Biol Chem 1991;266:15882–9.
4. Ludueña R, Roach M, Prasad V, Pettit G. Interaction of halichondrin B and homohalichondrin B with bovine brain tubulin. Biochem Pharmacol 1993;45:421–7.
5. Bai R, Cichacz Z, Herald C, Pettit G, Hamel E. Spongistatin 1 a highly cytotoxic sponge-derived marine natural product that inhibits mitosis microtubule assembly and the binding of vinblastine to tubulin. Mol Pharmacol 1993;44:757–66.
6. Hamel E. Natural products which interact with tubulin in the vinca domain maytansine rhizoxin phomopsin A dolastatins 10 and 15 and halichondrin B. Pharmacol Ther 1992;55:31–51.
7. Aicher T, Buszek K, Fang F, et al. Total synthesis of halichondrin B and norhalichondrin B. J Am Chem Soc 1992;114:3162–4.
8. Kishi Y, Fang FG, Forsyth C, Scola P, Yoon S. Halichondrins and related compounds. Washington, DC: U.S. Patent Office; 1995: U.S. Patent 5,436,238.
9. Stamos D, Sean S, Kishi Y. New synthetic route to the C14–C38 segment of halichondrins. J Org Chem 1997;62:7552–3.
10. Wang Y, Habgood G, Christ W, Kishi Y, Littlefield B, Yu M. Structure-activity relationships of halichondrin B analogues modifications at C30–C38. Bioorg Med Chem Lett 2000;10:1029–32.
11. Towle M, Salvato K, Budrow J, et al. In vitro and in vivo anticancer activities of synthetic macrocyclic ketone analogues of halichondrin B. Cancer Res 2001;61:1013–21.
12. Littlefield B, Palme M, Seletsky B, Towle M, Yu M, Zheng W. Macrocyclic analogs and methods of their use and preparation. Washington, DC: U.S. Patent Office; 2001: U.S. Patent 6,214,865.
13. Laemmli U. Cleavage of structural proteins during the assembly of the head of bacteriophage T4. Nature 1970;227:680–5.
14. Nicoletti I, Migliorati G, Pagliacci M, Grignani F, Riccardi C. A rapid and simple method for measuring thymocyte apoptosis by propidium iodide staining and flow cytometry. Immunol Methods 1991;139:271–9.
15. Goto H, Tomono Y, Ajiro K, et al. Identification of a novel phosphorylation site on histone H3 coupled with mitotic chromosome condensation. J Biol Chem 1999;274:25543–9.
16. Mantel CR, Gelfano VM, Kim YJ, et al. P21waf-1-Chk1 pathway monitors G1 phase microtubule integrity and is crucial for restriction point transition. Cell Cycle 2002;1:327–36.
17. Giannakakou P, Robey R, Fojo T, Blagosklonny MV. Low concentrations of paclitaxel induce cell type-dependent p53, p21 and G1/G2 arrest instead of mitotic arrest: molecular determinants of paclitaxel-induced cytotoxicity. Oncogene 2001;20:3806–13.
18. Blagosklonny MV, Schulte TW, Nguyen P, Mimnaugh EG, Trepel J, Neckers L. Taxol induction of p21WAF1 and p53 requires c-raf-1. Cancer Res 1995;55:4623–6.
19. Duke R, Cohen J. Morphological and biochemical assays of apoptosis. Curr Prot Immunol 1992;13:1713–6.
20. Mukhopadhyay D, Sundereshan S, Rao C, Karande A. Placental protein 14 induces apoptosis in T cells but not in monocytes. J Biol Chem 2001;276:28268–73.
21. Koopman G, Reutelingsperger C, Kuijten G, Keehnen R, Pals S, VanOers M. Annexin V for flow cytometric detection of phosphatidylserine expression on B cells undergoing apoptosis. Blood 1994;84:1415–20.
22. Vermes I, Haanen C, Steffens-Nakken H, Reutelingsperger C. A novel assay for apoptosis: flow cytometric detection of phosphatidylserine expression on early apoptotic cells using fluorescein labelled Annexin V. J Immunol Methods 1995;184:39–51.
23. Blagosklonny M, Giannakakou P, El-Deiry W, et al. Raf-1/bcl-2 phosphorylation a step from microtubule damage to cell death. Cancer Res 1997;57:130–5.
24. Halder S, Basu A, Croce C. Bcl-2 is the guardian of microtubule integrity. Cancer Res 1997;57:229–33.
25. Wang L, Liu XM, Kreis W, Budman D. The effect of antimicrotubule agents on signal transduction pathways of apoptosis: a review. Cancer Chemother Pharmacol 1999;44:355–61.
26. Srivastava R, Mi Q, Hardwick J, Longo D. Deletion of the loop region of Bcl-2 completely blocks paclitaxel-induced apoptosis. Proc Natl Acad Sci USA 1999;96:3775–80.
27. Yamamoto K, Ichijo H, Korsmeyer S. BCL-2 is phosphorylated and inactivated by an ASK1/Jun N-terminal protein kinase pathway normally activated at G2/M. Mol Cell Biol 1999;19:8469–78.
28. Liu X, Kim C, Yang J. Induction of apoptotic program in cell-free extracts: requirement for dATP and cytochrome C. Cell 1996;86:147–57.
29. Kluck R, Bossy-Wetzel E, Green D, Newmeyer D. The release of cytochrome C from mitochondria a primary site for Bcl-2 regulation of apoptosis. Science 1997;275:1132–6.
30. Zou H, Li Y, Liu X, Wang X. An APAF-1 cytochrome c multimeric complex is a functional apoptosome that activates procaspase-9. J Biol Chem 1999;274:11549–56.
31. Saleh A, Srinivasula S, Acharya S, Fishel R, Alnemri E. Cytochrome C and dATP-mediated oligomerization of Apaf-1 is a prerequisite for procaspase-9 activation. J Biol Chem 1999;274:17941–5.
32. Thornberry N, Lazebnik Y. Caspases: enemies within. Science 1998;281:1312–6.
33. Salvesen G, Dixit V. Caspases: intracellular signaling by proteolysis. Cell 1997;91:443–6.
34. Kuida K. Caspase-9. Int J Biochem Cell Biol 2000;32:121–4.
35. Portera A, Jänicke R. Emerging roles of caspase-3 in apoptosis. Cell Death Differ 1999;6:99–104.
36. Ozoren N, Kim K, Burns T, Dicker D, Moscioni A, El-Deiry W. The caspase 9 inhibitor Z-LEHD-FMK protects human liver cells while permitting death of cancer cells exposed to tumor necrosis factor-related apoptosis-inducing ligand. Cancer Res 2000;60:6259–65.
37. Kaufmann S, Desnoyers S, Ottaviano Y, Davidson N, Poirer G. Specific proteolytic cleavage of poly(ADP-ribose) polymerase: an early marker of chemotherapy-induced apoptosis. Cancer Res 1993;53:3976–85.
38. Smulson M, Simbulan-Rosenthal C, Boulares A, et al. Roles of poly(ADP-ribosyl)ation and PARP in apoptosis, DNA repair, genomic stability, and functions of p53 and E2F-1. Adv Enzyme Regul 2000;40:183–215.
39. Towle MJ, Salvato KA, Budrow J, et al. In vivo anticancer activity of synthetic halichondrin B macrocyclic ketone analogs ER-076349 and ER-086526 correlates with ability to induce irreversible mitotic blocks [abstract]. Proc Am Assoc Cancer Res 2001;42:367.
40. Fan M, Du L, Stone A, Gilbert K, Chambers T. Modulation of mitogen-activated protein kinases and phosphorylation of Bcl-2 by vinblastine represent persistent forms of normal fluctuations at G2–M. Cancer Res 2000;60:6403–7.
41. Bergamaschi D, Ronzoni S, Taverna S, et al. Cell cycle perturbations and apoptosis induced by isohomohalichondrin B (IHB), a natural marine compound. Br J Cancer 1999;79:267–77.
42. Haldar S, Jena N, Croce C. Inactivation of Bcl-2 by phosphorylation. Proc Natl Acad Sci USA 1995;92:4507–11.
43. Haldar S, Chintapalli J, Croce C. Taxol induces bcl-2 phosphorylation and death of prostate cancer cells. Cancer Res 1996;56:1253–5.
44. Blagosklonny M. Unwinding the loop of Bcl-2 phosphorylation. Leukemia 2001;15:869–74.
45. Haldar S, Basu A, Croce C. Bcl-2 is the guardian of microtubule integrity. Cancer Res 1997;57:229–33.
46. Blagosklonny M, Bishop P, Robey RT, Bates S. Loss of cell cycle control allows selective microtubule-active drug-induced Bcl-2 phosphorylation and cytotoxicity in autonomous cancer cells. Cancer Res 2000;60:3425–8.
47. Blagosklonny MV, Robey R, Sheikh MS, Fojo T. Paclitaxel-induced FasL-independent apoptosis and slow (non-apoptotic) cell death. Cancer Biol Ther 2002;1:113–7.
48. Broker LE, Huisman C, Ferreira CG, Rodriguez JA, Kruyt FA, Giaccone G. Late activation of apoptotic pathways plays a negligible role in mediating the cytotoxic effects of discodermolide and epothilone B in non-small cell lung cancer cells. Cancer Res 2002;62:4081–8.